International Journal of Applied Power Engineering (IJAPE)
Vol. 15, No. 2, June 2026, pp. 770~780
ISSN: 2252-8792, DOI: 10.11591/ijape.v15.i2.pp770-780

Comparative analysis of PM6:L8-BO organic and inverted organic solar cell

Karthika Krishnakumar[1], Ashish Grover[2], Pardeep Kumar[3]
[1]Department of Electronics and Communication Engineering, MRIIRS, Faridabad, India
[2]Department of Electrical and Electronics Engineering, MRIIRS, Faridabad, India
[3]Department of Applied Sciences, MRIIRS, Faridabad, India

Article Info

Article history:

Received Jul 11, 2025
Revised Jan 23, 2026
Accepted Mar 12, 2026

Keywords:

Inverted structure
Non fullerene acceptor
OghmaNano
Organic solar cell
PM6:L8-BO

ABSTRACT

Advancements in solar technologies are driven by the pursuit of higher efficiency and reduced environmental impact. This study presents a comprehensive and comparative analysis of organic and inverted organic solar cells (OSC and IOSC), using the OghmaNano software for simulations and analysis. This work is specifically designed to compare conventional and inverted structures and understand how device engineering impacts performance metrics. When OSCs are characterized by a low work-function cathode on top, IOSCs feature a clear conductive oxide cathode at the bottom. The study focusses on extracting key electrical output, including short circuit current density (J_{SC}), open-circuit voltage (V_{OC}), fill factor (FF) and power conversion efficiency (PCE), through the calculated current-voltage characteristic (J-V). Various physical characteristics, such as thickness of different layers and materials deployed as electron transport layer (ETL) and hole transport layer (HTL), are systematically investigated. Diverse top and bottom electrodes, encompassing monothin and multithin layer configurations, are proposed. The study shows that IOSC achieves higher efficiency than OSC, reaching 21.60%, while using a multithin layer ZTZ (ZnO/TiOx/ZnO) as the bottom contact, demonstrating improved charge transport and overall efficiency.

Corresponding Author:

Karthika Krishnakumar
Department of Electronics and Communication Engineering, MRIIRS
Faridabad, Haryana, India
Email: karthikakrishnakumar18752@gmail.com

1. INTRODUCTION

The conjugated polymer-based organic solar cells (OSCs) are being investigated as a substitute for inorganic solar cells due to their inexpensiveness, pliability, lightweight, and depositing ability using the room temperature solution technique [1], [2]. Despite these advantages, investigation on OSCs faces significant hurdle regarding their widespread commercialization due to poor power conversion efficiency (PCE) [3]. To break through this efficiency ceiling, the OSC community has witnessed an upsurge in interest and research into non-fullerene acceptors (NFA) since 2015 [4]. NFAs have become a cornerstone for next-generation OSCs due to their enhanced electron mobility, tunable absorption spectra enabling better use of solar spectrum, and superior donor-acceptor miscibility which optimizes the blend morphology [5], [6]. So, ongoing efforts are focused on improving PCE of NFA based OSC through the utilization of innovative materials and device architectures both through simulation and experimentation. Experiments to assess the performance of OSCs are difficult, expensive, and time-consuming. Computer simulation is more practical while conducting research on OSC in its early phases. By computer simulations, we can create and optimize our own OSC structure, test different materials, and make adjustments without consuming a lot of resources

or going over budget before trying it out in actual experiments. Software tools such as OghmaNano, MATLAB, 1D Amps, PC1D, matrix transfer scaps-1D, are widely used for simulating OSCs.

The core structure of OSCs involve a transparent substrate coated with a transparent conductive electrode substance, commonly indium tin oxide (ITO), forming the basis for both conventional and inverted structures [7]. ITO has strong electrical conductivity and outstanding transparency [7]. Standard OSC structure consists of anode, hole transport layer (HTL), active layer, electron transport layer (ETL), and cathode whereas IOSC structure consists of anode, ETL, active layer, HTL, and cathode, in order [8]. In the standard OSC structure, usually a low work function metal is used as cathode. This structure experiences low air stability of low work function metal cathode and high acidity of interfacial layer. For eradicating this shortcoming, IOSC structure was developed, with air-stable high-work-function electrode material, such as silver or gold, as cathode [9], [10].

While doing literature study, it has been significantly noticed that the ongoing academic research focused on studies exclusively either on OSC based or IOSC based structures. Evaluation of the comparative performances of OSC and IOSC with non-fullerene materials in the active layer are noticeably lacking. Hence to redress such lacking, this research aims to compare the electrical characteristics of PM6:L8-BO based OSC and IOSC, by analyzing the impact of active layer thickness, ETL thickness, HTL thickness, ETL materials and HTL materials on electrical outputs and enhancing charge collection using multi thin layer electrodes instead of monolayers. Here we use OghmaNano 8.0.041 version software to numerically simulate OSC structure with ITO/Pedot:Pss/PM6:L8-BO/TiOx /Al and IOSC structure with ITO/TiOx/PM6:L8-BO/Pedot:Pss/Ag as shown in Figure 1.

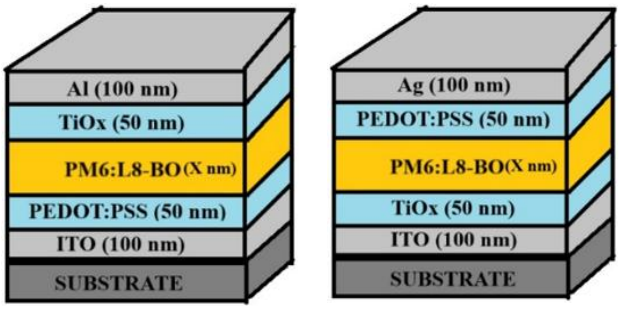

Figure 1. Proposed structure in simulation: (a) OSC and (b) IOSC

2. METHOD

Since organic semiconductors have an amorphous structure, an important aspect of their transport mechanism of optoelectronic characteristics is their density of states (DoS) [11]. This might make it more difficult to comprehend the physical processes that occur [12]. The OghmaNano 8.0.041 version software was deployed to conduct the electrical simulation [13]. The finite-difference drift-diffusion model is used by this program for carrier trapping, detrapping, and transit [14].

2.1. Transport model

The band gap energy of the bulk hetero junction (BHJ) material is defined by the n-type lowest unoccupied molecular orbital (LUMO) and p-type highest occupied molecular orbital (HOMO) energies, which are considered while modelling free carrier transport [15]. The LUMO level in organic materials is comparable to that of E_c, while the HOMO level is equivalent to the E_v energy band gap edge. The easiest way to simulate the BHJ is to use an analogous layer with an equivalent band gap energy located between the p-type HOMO and the n-type LUMO levels. This is because the BHJ is a combination of n-type and p-type zones. The internal potential distribution φ is then obtained by solving the Poisson equation [14].

$$\frac{d}{dx}.\varepsilon_0\varepsilon_r\frac{d\varphi}{dx} = qn_f - p_f + n_t - p_t \quad (1)$$

Where q: charge on electron, ε_0: permittivity of free space, ε_r: permittivity of active layer, n_f: electron density, p_f: hole density, and n_t, p_t: trapped charge density [13]. The formulas for calculating the continuance of electron and hole currents in a 1D steady-state scenario are found in MacKenzie [13].

$$\frac{\partial J_n}{\partial x} = q(R_e - G) \tag{2}$$

$$\frac{\partial J_p}{\partial x} = q(R_h - G) \tag{3}$$

Where $R_{e,h}$: recombination rate of free carriers and G: generation rate of free carriers [13].

The electron current flux density (J_n) and the hole current flux density (J_p) may be found by solving these equations [14]. For free carriers, Maxwell-Boltzmann statistics are assumed.

$$J_n = q\mu_e n_f \frac{\partial E_{LUMO}}{\partial x} + qD_n \frac{\partial n_f}{\partial x} \tag{4}$$

$$J_p = q\mu_p p_f \frac{\partial E_{HOMO}}{\partial x} + qD_p \frac{\partial P_f}{\partial x} \tag{5}$$

$$E_{LUMO} = -\chi - q\phi \;\; E_{HOMO} = -\chi - E_g - q\phi, \chi = LUMO\ mobility\ edge - vaccum\ level$$

Where $D_{n,p}$: electron and hole diffusion coefficients, E_g: HOMO-LUMO, and ϕ: built in potential of the device [14].

2.2. Trapping and recombination mechanisms of carriers

Numerous energy levels in disordered organic semiconductors are in close proximity to the HOMO and LUMO energies [16]. This disorder produces a variety of localized gap states with varying energy that are produced by this disorder [17]. Furthermore, the distribution of trap-like defect states is tail-shaped [18].

The distribution of traps in a polymeric substance is closely associated to the processes of trapping and de-trapping. Charge injection, trapping, and de-trapping are the three primary phases of the trapping model [19]. There are two types of defects viz. chemical and physical defects. Differences in morphological crystallinity, microstructure, and molecular weight lead to physical flaw [19], [20]. On the other hand, photo-oxidation leads to chemical flaws, which change the chemical structure of the material [19], [20]. Chemical faults have been shown to be related to deep traps, while physical faults are linked to shallow traps.

Although the DoS is often associated with the Gaussian form, it is important to remember that an exponential DoS or a mix of Gaussian and exponential distributions is also possible. Two Gaussians revolving around the LUMO and HOMO levels comprise an alternative model. Recently the Shockley–Read–Hall (SRH) recombination model has been applied in organic photovoltaics (OPVs). This model is similar to the Langevin recombination model with carrier traps in that which describes the recombination of carriers changing from free to trapped states in a steady state [19], [20].

The structure of the DoS over the gap energy and the corresponding recombination and trapping process are depicted in Figure 2. This study examines a model made up of exponentially decaying tail states (DoS) that serve as free carrier trap states. Furthermore, the parabolic bands characterized by LUMO energy as electron minima and HOMO energy as hole maxima explain the carrier extended states [14].

The SRH recombination model explains carrier trapping and recombination by describing the movement of carriers from free to confined states for both electrons and holes. MacKenzie [13] provides the equation that determines the balance of the carriers for each trap level.

$$\frac{\delta n_t}{\delta t} = r_{ec} - r_{ee} - r_{hc} + r_{he} \tag{6}$$

Where n_t: trapped electrodensity and r_{ec}, r_{ee}, r_{hc}, r_{he}: electron and hole capture rate, escape rate [13].

$$\begin{aligned} r_{ec} &= nv_{th}\sigma_n N_t(1-f) \\ r_{ee} &= e_p N_t f \\ r_{hc} &= pv_{th}\sigma_p N_t f \\ r_{he} &= e_p N_t(1-f) \\ \frac{\partial p_t}{\partial t} &= r_{hc} - r_{he} - r_{ec} - r_{ee} \end{aligned} \tag{7}$$

Where e_n, e_p: electron and hole escape rate.

$$e_n = v_{th}\sigma_n N_c exp\frac{E_t - E_c}{KT} \tag{8}$$

$$e_p = v_{th}\sigma_p N_v exp\frac{E_V - E_t}{KT} \tag{9}$$

Where V_{th}: thermal emission velocity of carriers, $\sigma_{n,p}$: trap cross sections, $N_{c,v}$: effective density of states for free carriers, f: Fermi-Dirac occupation function, and N_t: trap density of exponential tail distribution [13], [14].

$$N_t(E) = \frac{\int_{E-\Delta E/2}^{E+\Delta E/2} N^{e/h} exp\,(E/E_U^{e/h}) dE}{\Delta E} \quad (10)$$

$E_U^{e/h} = Tail\ slope\ energy\ characteristic$
$N^{e/h} = trap\ density\ at\ LUMO(HOMO) band\ edges$

The DoS parameters are shown in Table 1 [14], [21]. OSC and IOSC are numerically simulated at 300K with the AM1.5 spectrum. The software database contains the input parameters for all materials used in this work. The key electrical outputs of the solar cells are derived from the J-V characteristics found in the calculations. These outputs consist of the PCE, FF, V_{OC}, and J_{SC}.

2.3. Model calibration

To calibrate the model, the simulation and experimental study in the cited Zhu *et al*. [22] was referred. From Zhu *et al*. [22], it is noted that simulation and experimental outcomes were in close agreement. To validate the model further, here the simulation as cited in Zhu *et al.* [22] was reproduced. The reproduced results, as depicted in Figure 3 and Table 2, show close agreement with both the original simulation and the experimental findings outlined in Zhu *et al.* [22]. This alignment demonstrated the successful calibration of the model.

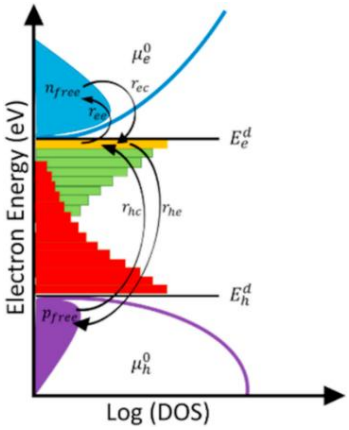

Figure 2. DoS of PM6:L8-BO [14]

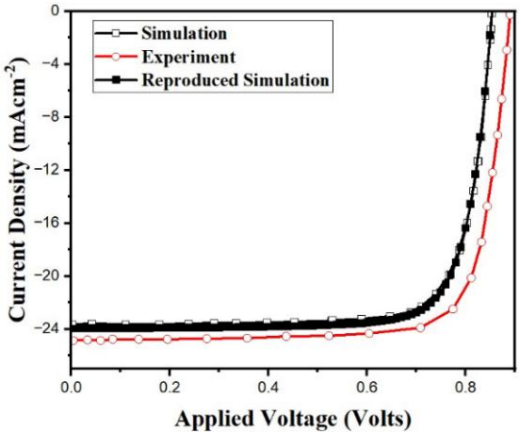

Figure 3. Comparison of reproduced J-V curve with simulated and experimental results reported in [22]

Table 1. Dos parameters

Materials	PM6:L8-BO	
Electrical parameters	Values	Unit
Electron trap density	3.8000e26	m^3eV^{-1}
Trapped hole to free electron	2.5000e-20	m^{-2}
Hole trap density	1.4500e25	m^3eV^{-1}
Free electron to trapped electron	2.5000e-20	m^{-2}
Electron tail slope	0.04	eV
Trapped electron to free hole	1.3200e-22	m^{-2}
Hole tail slope	0.06	eV
Free hole to trapped hole	4.8600e-22	m^{-3}
Electron mobility	2.48e-06	$m^2V^{-1}s^{-1}$
Effective density of free hole states	2.8600e25	m^{-3}
Hole mobility	2.48e-06	$m^2V^{-1}s^{-1}$
Relative permittivity	3.8	Au
Effective density of free electron states	1.2800e27	m^{-3}
Recombination rate constant	0.0	m^3s^{-1}
Affinity	3.8	eV
Gap energy	1.46	eV

Table 2. Comparison table

Findings	PCE (%)	JSC ($mAcm^{-2}$)	VOC (V)	FF (%)
Zhu *et al.* [22] simulation	16.1	24.0	0.853	78
Zhu *et al.* [22] experiment	18.2	25.7	0.888	79.9
Reproduced simulation (this work)	16.07	23.95	0.853	78

3. RESULTS AND DISCUSSION

The key performance parameters that determine the PCE of the solar cell are summarized below. Each parameter reflects a different aspect of device operation, and collectively they provide insight into the factors limiting efficiency. A brief explanation of these parameters is provided before discussing the results in detail: i) V_{OC}: which is the energy level difference between the potential in the region where the free electrons are the majority and the region where the free holes are the majority and ii) J_{SC}: The number of photogenerated carriers produced in the active layer during illumination and the efficiency with which charges are separated throughout the photoactive layer are the two main factors that define the quantity of J_{SC}. Hence, J_{SC} may be changed by adjusting the active layer thickness or by changing the structure that results in the lowest usable bandgap [8], [11], [23].

$$FF: \frac{V_m \times I_m\ (maximum\ power\ point)}{Jsc \times Voc}$$

Shunt resistance, series resistance, and the rate at which charge recombines or is extracted from the solar cell are some of the elements that influence the FF. These factors have a substantial impact on the quality of the cell and are entirely related to the V_{OC}, J_{SC}, and active layer morphology [8], [11], [23].

$$PCE: Voc \times Jsc \times FF \tag{11}$$

3.1. Layer thickness impact: OSC and IOSC comparison

3.1.1. Impact of active layer thickness

Each of the layers of the BHJ device is layered on top of one another. It is difficult to enhance the device performance because of phenomena such as reflections and interferences in the layers. It is crucial to consider the thickness of the PM6:L8-BO, which is the main layer [24]. We examine its thickness because it determines the amount of light that the device can absorb. Additionally, the exciton production of the thickness determines the primary layer, which is crucial for the device [24].

An optimization of BHJ structures was carried out in an extensive study. The active layer (PM6:L8-BO) thickness was varied throughout the investigation between 100 and 500 nm. Figure 4(a) displays the J-V curves, and Figure 4(b) shows electrical outputs for various PM6:L8-BO thicknesses. Interestingly, the J-V properties are quite responsive to variations in the active layer thickness. The J_{SC} is directly linked to the absorption capacity of the active layer, as was previously noted. The findings show a clear correlation between J-V characteristics and active layer thickness. Significant variations in J_{SC}, PCE, and FF are observed for both OSC and IOSC as the thickness of the PM6:L8-BO increases, according to observations from Figure 4(b). V_{OC}, seems less susceptible to changes in thickness. Diffusion length and absorption have an impact on J_{SC}, which is associated with carrier photogeneration and transportation. In OSC and IOSC, the optimal J_{SC} thickness is around 200 nm and 250 nm. The maximum current at a given thickness indicates an excessive exciton route at higher thicknesses and inadequate absorption at lower thicknesses. Smaller thicknesses of 150 nm for OSC and 100 nm for IOSC yield a PCE of 17.43% and 19.95%, respectively. Due to series resistance, FF reduces as the thickness of the active layer increases, while V_{OC} marginally decreases in both devices from 1.03 to 0.99 V. The efficiency peak occurs at a thickness less than that of the current due to different trends in FF and J_{SC}. There was some improvement, as the J_{SC} in IOSC was better than in OSC. This distinction can be attributed to variations in light transmission and absorption mechanisms between the two configurations. In the OSC structure, light traverses the layers sequentially: ITO, PEDOT:PSS, and then finally reaches PM6: L8-BO. In contrast, in IOSC, the sequence is reversed, where light first passes through TiOx before reaching PM6:L8-BO. The energy gaps of the different materials have an impact on this performance disparity. Compared to PEDOT:PSS, which has an energy gap of 1.7 eV, TiOx in IOSC, which has a gap of 3.2 eV, is more transparent to visible light. Furthermore, the study considers the absorption properties, which are more efficient than the p-component [25].

3.1.2. Impact of ETL thickness

The buffer layers, ETL and HTL, are acting as exciton blocking layers (EBL) and to get more carriers into and out of the device [12]. The primary objective of this section is to analyze the impact of ETL

thicknesses on OSC and IOSC performance. For OSC and IOSC, the PM6:L8-BO maintained an ideal thickness of 150 nm and 100 nm, respectively. TiOx was chosen as the first ETL material, and its thickness ranges from 10 nm to 50 nm. The resultant J-V characteristics are illustrated in Figure 5(a), which sheds light on how the device's performance is affected by the thickness of the ETL. Figure 5(b) shows the electrical outputs that were extracted. It also shows how the changes in J_{SC} and PCE are comparable. There are parallels between the PCE and J_{SC} variations in OSC and IOSC. Changes in ETL thickness have a remarkable impact on OSC performance. In OSC, J_{SC} and PCE increases from 21.27 to 21.71 $mAcm^{-2}$ and from 17.20 to 17.43%, respectively. J_{SC} and PCE are higher in IOSC, but do not significantly change as the thickness of the ETL increases. Additionally, V_{OC} and FF show very minor variations on both devices. The results align with previous findings showing an influence of variation in ETL thickness on OSC [25]-[29]. The observed performance difference may be attributed to the positioning of the ETL in the OSC, situated at the top, just below the cathode. With illumination provided from the bottom, the OSC benefits from improved photocurrent. Achieving this enhancement involved the strategic insertion of TiOx as an optical spacer between the BHJ layer and the Al metal electrode. The insertion of TiOx optimizes light absorption within the OSC structure, thereby increasing the photocurrent and contributing to the superior performance observed in the OSC.

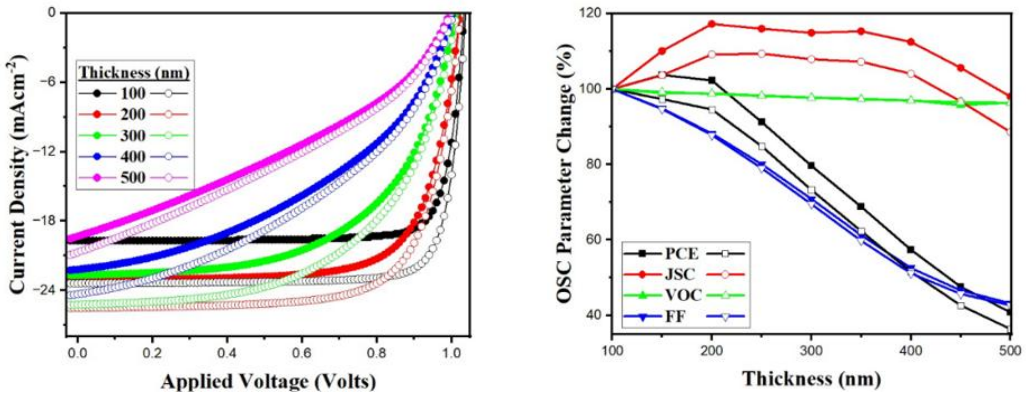

Figure 4. Active layer thickness OSC (solid) IOSC (hollow): (a) J-V characteristics and (b) extracted electrical outputs

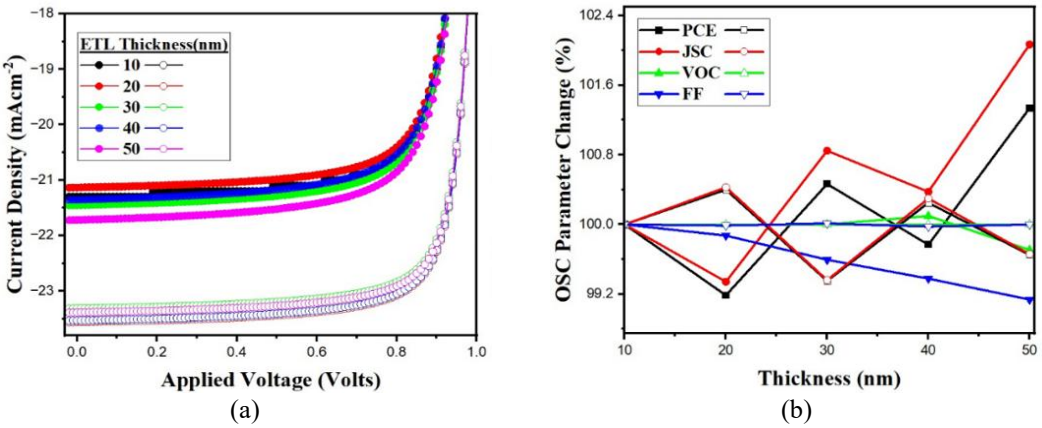

Figure 5. ETL thickness impact on OSC (solid) IOSC (hollow): (a) J-V characteristics and (b) extracted electrical outputs

3.1.3. Impact of HTL thickness

The study now focusses on the impact of the HTL thickness. The active layer and ETL thicknesses are 150 nm and 50 nm for OSC, and 100 nm and 20 nm for IOSC. PEDOT:PSS has been selected as the HTL material, and its thickness ranges from 10 to 50 nm. The resulting J-V characteristics are provided in Figure 6(a), and the extracted electrical outputs are illustrated in Figure 6(b). In each case, specific thickness values were selected according to the best efficiency. In OSC, a slight drop is there in PCE and J_{SC} with

increasing HTL thickness. This finding is consistent with the research reported in [27]-[29]. IOSC exhibits a little decline from the peak values and does not demonstrate a strong correlation between changes in J_{SC} and PCE. HTL thickness has very little influence overall, and both V_{OC} and FF in IOSC are basically unaffected. The low hole (majority carriers) mobility in this area is responsible for this discovery, which also explains why there is not much of an impact on these electrical outputs.

3.2. Impact of different ETL materials on photovoltaic performance

The several materials used in OSCs as the ETL, are examined in this section. ETL is an essential component that is positioned between the Al cathode and PM6:L8-BO in OSC and between ITO cathode and PM6:L8-BO in IOSC. Important requirements for quality ETL content: should make electron conduction easier, serve as a layer that blocks holes, enabling only electrons to transit to the cathode, and increase the spatial distribution of light by forming a barrier in the photoactive layer through back reflection [30], [31]. The goal of this section is to determine which material best satisfies these requirements to achieve the best possible performance from solar cells. The materials proposed for this study include V_2O_5, ZnO, and TiOx. The recovered output parameters are provided in Table 3, and the resultant J-V characteristics are shown in Figure 7(a). It is obvious that the best ETL material for OSC is ZnO. ZnO appears to be more suitable as it has a wider energy band gap, which improves light transmission. Its affinity to ITO aligns well with the requirements of the device. TiOx is better suited for IOSC, where the cathode is simple metal (Al) and the ETL is located at the back, because of its suitability for electron injection and collection in these particular circumstances.

3.3. Impact of different HTL materials on photovoltaic performance

The following are the selected HTL materials from other publications in this section: CU2O, P3HT, and PEDOT:PSS. Table 4 lists the recovered electrical outputs, and Figure 7(b) shows the J-V characteristics. Cu2O, the HTL with the best performance in OSC, yields a PCE of 20.12%. Cu2O ensures effective light transmission due to its high band gap energy, strategically positioned on the illuminated substrate side (ITO). The improved performance is due to a larger energy barrier between the PM6:L8-BO LUMO level and the HTL conduction band. Furthermore, the improved alignment of the PM6:L8-BO HOMO level with the HTL valence band improves hole collection and electron blocking at the interface. CU2O produces an optimal efficiency of 21.21% in IOSC, ascribed to the high work function of PEDOT:PSS, efficient hole transport, high electrical conductivity, transparency in the visual range, and excellent matching with the HOMO level of frequently employed donor polymers [32].

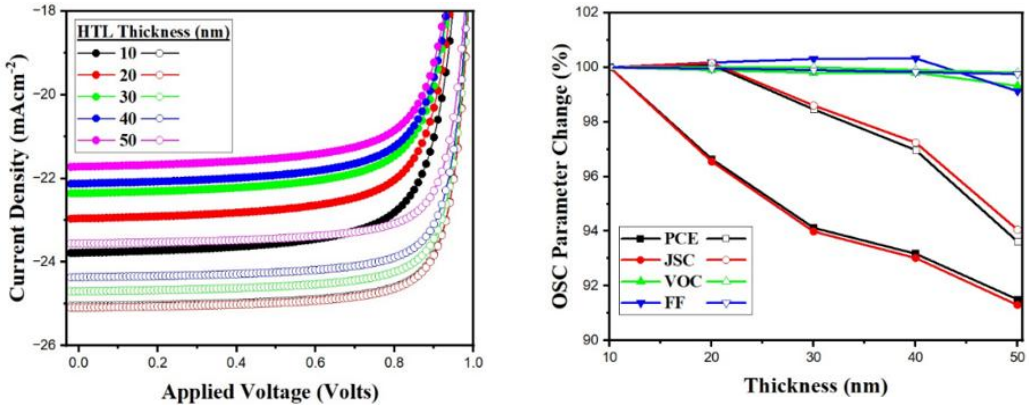

(a) (b)

Figure 6. HTL thickness impact on OSC (solid) IOSC (hollow): (a) J-V characteristics and (b) extracted electrical outputs

Table 3. Impact of different ETL materials on photovoltaic performance

Parameters		Voc (V)	Jsc (mA/cm2)	FF (%)	PCE (%)
OSC	TiOx	1,029	23.78	77.85	19.05
	ZnO	1,029	23.87	77.89	19.13
	V2O5	1,027	22.31	78.30	17.94
IOSC	TiOx	1,039	25.09	82.40	21.49
	ZnO	1,039	24.99	82.41	21.41
	V2O5	1,027	15.60	83.34	13.35

Table 4. Impact of different HTL materials on photovoltaic performance

Parameters		Voc (V)	Jsc (mA/cm2)	FF (%)	PCE (%)
OSC	PEDOT:PSS	1,029	23.87	77.89	19.13
	CU2O	1,030	25.13	77.70	20.12
	P3HT	1,027	22.88	78.06	18.36
IOSC	PEDOT:PSS	1,039	25.09	82.40	18.61
	CU2O	1,039	24.77	82.39	18.93
	P3HT	1,039	24.32	82.46	18.82

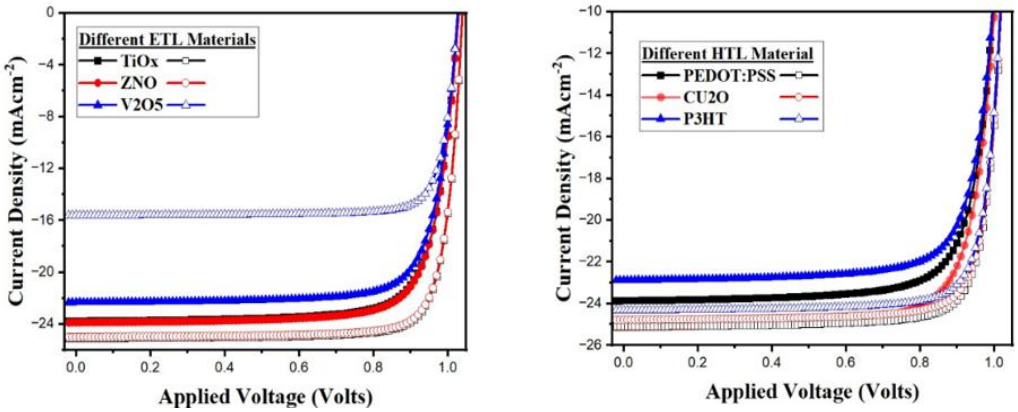

Figure 7. J-V characteristics of OSC (solid) and IOSC (hollow): different (a) ETL materials and (b) HTL materials

3.4. Impact of multilayer on photovoltaic performance

In earlier parts, ITO was deployed as substrate, acting as the bottom electrode while the top electrode was a simple metal. Various studies have offered that cell performance can be improved by using multilayer electrodes in place of single layer electrodes and by adjusting their ETL (or HTL) [33]. In this stage, the top electrode metals, Al for OSC and Ag for IOSC, are kept, while multilayer electrodes are introduced at the bottom, facing the light. Simplified depictions of OSC and IOSC using the suggested multilayer electrodes are illustrated in Figures 8(a) and 8(b).

3.4.1. TCO/TiOx/ZNO as bottom electrode

The first oxide layer is FTO, whereas the thicknesses of the TiOx and ZnO layers remain fixed at 50 nm (OSC) and 20 nm (IOSC). Thinner FTO has less effect on light absorption. Substitute oxides such as ITO and ZnO are used in place of the FTO material. For OSC and IOSC, J-V characteristics are depicted in Figure 9, and figures of merit are compiled in Table 5. ZnO increases OSC and IOSC efficiency to 19.00% and 21.60%, respectively. In OSC, electron collection is solely controlled by energy level alignment at the top, while effective transmission at the bottom is crucial. In contrast to IOSC, where hole collection at the top is slower, OSC electron collection is more sensitive to top electrode parameters because electrons have greater mobility than holes.

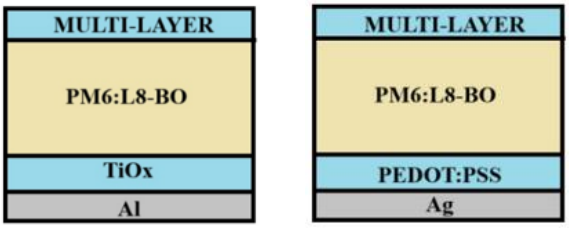

Figure 8. Simulated multilayered bottom electrode structure: (a) OSC and (b) IOSC

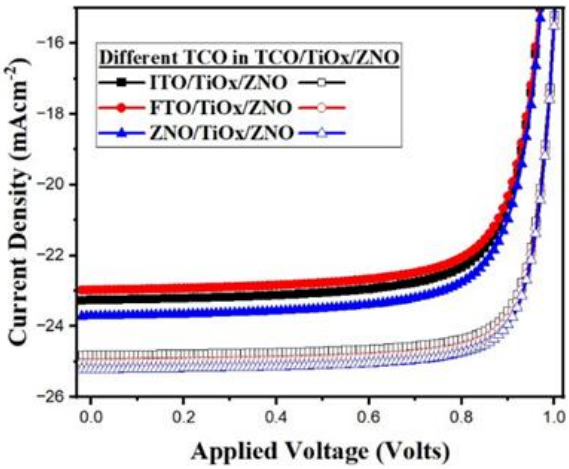

Figure 9. J-V characteristics of different TCO in TCO/TiOx/ZNO

Table 5. Effect of different TCO in TCO/TiOx/ZnO

Structure	Electrodes	Voc (V)	Jsc (mA/cm2)	FF (%)	PCE (%)
OSC	FTO/TiOx/ZnO	1,028	23.97	78.03	18.42
	ITO/TiOx/ZnO	1,028	22.25	77.98	18.65
	ZnO/TiOx/ZnO	1,028	23.70	77.90	19.00
IOSC	FTO/TiOx/ZnO	1,039	25.03	82.41	21.44
	ITO/TiOx/ZnO	1,039	24.79	82.43	21.24
	ZnO/TiOx/ZnO	1,039	25.21	82.38	21.60

4. CONCLUSION

In conclusion, this research, conducted using OghmaNano software, aimed to comprehensively explore the electrical parameters of OSC and IOSC featuring the active layer PM6:L8-BO. The investigation covered a range of variables, including active layer thickness, ETL and HTL characteristics, and the use of multi-thin layer electrodes for simulations. These analyses provided crucial insights into the factors influencing the performance of OSC and IOSC. The study revealed that the thickness of the active layer significantly affects PM6:L8-BO-based OSC and IOSC, while the ETL and HTL thicknesses and materials play vital roles. The choice of ETL material demonstrated a notable impact on both OSC and IOSC, whereas the HTL material had a minor influence on IOSC. Moreover, the study introduced a TCO/TiOx/ZNO multi-thin layer as a bottom electrode. Efficiency highlights showcased the most effective OSC configuration, achieving an efficiency of 20.12% with the ITO/CU2O/PM6:L8-BO/ZnO/Al structure. Another configuration, employing the ZTZ/PM6:L8-BO/ZnO/Al structure with ZTZ as a tri-layer bottom electrode, demonstrated a slightly lower efficiency of 19%. IOSC configuration, achieving an efficiency of 21.43% with the Ag/PEDOT:PSS/PM6:L8-BO/TiOx/ITO structure. Another configuration, employing the Ag/PEDOT:PSS/PM6:L8-BO/ZTZ structure with ZTZ as a tri-layer bottom electrode, demonstrated a slightly lower efficiency of 21.60%. The research suggests that exploring alternative materials, instead of ZTZ, holds promise for enhancing efficiency. While these findings contribute valuable insights, it's essential to recognize certain limitations. Further study is needed to resolve these limitations and broaden the application of the existing findings. As a whole, this study expands our knowledge of OSC and IOSC performance and offers avenues for future research and practical applications in the field of OSCs.

FUNDING INFORMATION

Authors state no funding involved.

AUTHOR CONTRIBUTIONS STATEMENT

This journal uses the Contributor Roles Taxonomy (CRediT) to recognize individual author contributions, reduce authorship disputes, and facilitate collaboration.

Name of Author	C	M	So	Va	Fo	I	R	D	O	E	Vi	Su	P	Fu
Karthika Krishnakumar	✓	✓	✓	✓	✓	✓	✓	✓	✓	✓	✓		✓	
Ashish Grover	✓	✓								✓		✓		
Pardeep Kumar	✓	✓								✓		✓		

C : **C**onceptualization
M : **M**ethodology
So : **So**ftware
Va : **Va**lidation
Fo : **Fo**rmal analysis
I : **I**nvestigation
R : **R**esources
D : **D**ata Curation
O : Writing - **O**riginal Draft
E : Writing - Review & **E**diting
Vi : **Vi**sualization
Su : **Su**pervision
P : **P**roject administration
Fu : **Fu**nding acquisition

CONFLICT OF INTEREST STATEMENT

Authors state no conflict of interest.

DATA AVAILABILITY

This study is based on computational simulations. All relevant simulation parameters and methodological details are provided within the article. Additional data can be made available by the corresponding author upon reasonable request.

REFERENCES

[1] D. Chen *et al.*, "Performance comparison of conventional and inverted organic bulk heterojunction solar cells from optical and electrical aspects," *IEEE Transactions on Electron Devices*, vol. 60, no. 1, pp. 451–457, Jan. 2013, doi: 10.1109/TED.2012.2224114.

[2] I. Malti, A. Chiali, and N. C. Sari, "Numerical study of electrical behavior of P3HT/PCBM bulk heterojunction solar cell," *Applied Solar Energy*, vol. 52, no. 2, pp. 122–127, Apr. 2016, doi: 10.3103/S0003701X16020195.

[3] C. J. Brabec, "Organic photovoltaics: technology and market," *Solar Energy Materials and Solar Cells*, vol. 83, no. 2–3, pp. 273–292, Jun. 2004, doi: 10.1016/j.solmat.2004.02.030.

[4] Y. Lin *et al.*, "A simple n-dopant derived from diquat boosts the efficiency of organic solar cells to 18.3%," *ACS Energy Letters*, vol. 5, no. 12, pp. 3663–3671, Dec. 2020, doi: 10.1021/acsenergylett.0c01949.

[5] Y. Li *et al.*, "Recent progress in organic solar cells: a review on materials from acceptor to donor," *Molecules*, vol. 27, no. 6, p. 1800, Mar. 2022, doi: 10.3390/molecules27061800.

[6] H. Fu, Z. Wang, and Y. Sun, "Polymer donors for high-performance non-fullerene organic solar cells," *Angewandte Chemie International Edition*, vol. 58, no. 14, pp. 4442–4453, Mar. 2019, doi: 10.1002/anie.201806291.

[7] M. C. Scharber and N. S. Sariciftci, "Efficiency of bulk-heterojunction organic solar cells," *Progress in Polymer Science*, vol. 38, no. 12, pp. 1929–1940, Dec. 2013, doi: 10.1016/j.progpolymsci.2013.05.001.

[8] K. Krishnakumar, A. Grover, and P. Kumar, "Performance of multifarious active layer materials in organic photovoltaic cells: a review," *International Journal of Nanoelectronics and Materials (IJNeaM)*, vol. 16, no. 4, pp. 933–946, Oct. 2024, doi: 10.58915/ijneam.v16i3.1380.

[9] D. W. Zhao, P. Liu, X. W. Sun, S. T. Tan, L. Ke, and A. K. K. Kyaw, "An inverted organic solar cell with an ultrathin Ca electron-transporting layer and MoO3 hole-transporting layer," *Applied Physics Letters*, vol. 95, no. 15, Oct. 2009, doi: 10.1063/1.3250176.

[10] D. W. Zhao *et al.*, "Optimization of an inverted organic solar cell," *Solar Energy Materials and Solar Cells*, vol. 94, no. 6, pp. 985–991, Jun. 2010, doi: 10.1016/j.solmat.2010.02.010.

[11] N. K. Elumalai, C. Vijila, R. Jose, A. Uddin, and S. Ramakrishna, "Metal oxide semiconducting interfacial layers for photovoltaic and photocatalytic applications," *Materials for Renewable and Sustainable Energy*, vol. 4, no. 3, p. 11, Sep. 2015, doi: 10.1007/s40243-015-0054-9.

[12] S. Banerjee, S. K. Gupta, A. Singh, and A. Garg, "Buffer layers in inverted organic solar cells and their impact on the interface and device characteristics: An experimental and modeling analysis," *Organic Electronics*, vol. 37, pp. 228–238, Oct. 2016, doi: 10.1016/j.orgel.2016.06.031.

[13] R. C. I. MacKenzie, *Understanding gpvdm v7. 88+*. 2022.

[14] R. C. I. MacKenzie, C. G. Shuttle, M. L. Chabinyc, and J. Nelson, "Extracting microscopic device parameters from transient photocurrent measurements of P3HT:PCBM solar cells," *Advanced Energy Materials*, vol. 2, no. 6, pp. 662–669, Jun. 2012, doi: 10.1002/aenm.201100709.

[15] R. C. I. MacKenzie, T. Kirchartz, G. F. A. Dibb, and J. Nelson, "Modeling nongeminate recombination in P3HT:PCBM solar cells," *The Journal of Physical Chemistry C*, vol. 115, no. 19, pp. 9806–9813, May 2011, doi: 10.1021/jp200234m.

[16] S. R. Forrest, "The path to ubiquitous and low-cost organic electronic appliances on plastic," *Nature*, vol. 428, no. 6986, pp. 911–918, 2004, doi: 10.1038/nature02498.

[17] C.-X. Zhou, J.-X. Sun, Z.-J. Deng, and S. Zhou, "Study of applicability of Boltzmann-statistics and two mobility models for organic semiconductors," *Semiconductors*, vol. 47, no. 10, pp. 1351–1357, Oct. 2013, doi: 10.1134/S1063782613100291.

[18] S. Kugler, "What is the origin of tail states in amorphous semiconductors?," *Journal of Physics: Conference Series*, vol. 253, p. 012013, Nov. 2010, doi: 10.1088/1742-6596/253/1/012013.

[19] T. Zhou, G. Chen, R. Liao, and Z. Xu, "Charge trapping and detrapping in polymeric materials: trapping parameters," *Journal of Applied Physics*, vol. 110, no. 4, Aug. 2011, doi: 10.1063/1.3626468.

[20] N. Liu and G. Chen, "Changes in charge trapping/detrapping in polymeric materials and its relation with aging," in *2013 Annual Report Conference on Electrical Insulation and Dielectric Phenomena*, IEEE, Oct. 2013, pp. 800–803, doi: 10.1109/CEIDP.2013.6747077.

[21] C. Xiao *et al.*, "Hybrid cycloalkyl-alkyl chain-based symmetric/asymmetric acceptors with optimized crystal packing and interfacial exciton properties for efficient organic solar cells," *Advanced Science*, vol. 10, no. 7, Mar. 2023, doi: 10.1002/advs.202206580.
[22] L. Zhu *et al.*, "Single-junction organic solar cells with over 19% efficiency enabled by a refined double-fibril network morphology," *Nature Materials*, vol. 21, no. 6, pp. 656–663, Jun. 2022, doi: 10.1038/s41563-022-01244-y.
[23] D. H. Apaydın, D. E. Yıldız, A. Cirpan, and L. Toppare, "Optimizing the organic solar cell efficiency: role of the active layer thickness," *Solar Energy Materials and Solar Cells*, vol. 113, pp. 100–105, Jun. 2013, doi: 10.1016/j.solmat.2013.02.003.
[24] Y. Min Nam, J. Huh, and W. Ho Jo, "Optimization of thickness and morphology of active layer for high performance of bulk-heterojunction organic solar cells," *Solar Energy Materials and Solar Cells*, vol. 94, no. 6, pp. 1118–1124, Jun. 2010, doi: 10.1016/j.solmat.2010.02.041.
[25] P. D. Andersen, J. C. Skårhøj, J. W. Andreasen, and F. C. Krebs, "Investigation of optical spacer layers from solution based precursors for polymer solar cells using X-ray reflectometry," *Optical Materials*, vol. 31, no. 6, pp. 1007–1012, Apr. 2009, doi: 10.1016/j.optmat.2008.11.014.
[26] J. Gilot, I. Barbu, M. M. Wienk, and R. A. J. Janssen, "The use of ZnO as optical spacer in polymer solar cells: theoretical and experimental study," *Applied Physics Letters*, vol. 91, no. 11, Sep. 2007, doi: 10.1063/1.2784961.
[27] Y. Long, "Effects of metal electrode reflection and layer thicknesses on the performance of inverted organic solar cells," *Solar Energy Materials and Solar Cells*, vol. 94, no. 5, pp. 744–749, May 2010, doi: 10.1016/j.solmat.2009.12.017.
[28] K. Krishnakumar, A. Grover, and P. Kumar, "Device simulation of PTB7:PC70BM based plastic solar cells using oghmanano software," in *2023 IEEE IAS Global Conference on Renewable Energy and Hydrogen Technologies (GlobConHT)*, Mar. 2023, pp. 1–5, doi: 10.1109/GlobConHT56829.2023.10087535.
[29] K. Krishnakumar, A. Grover, and P. Kumar, "Efficiency enhancement of PM6:Y6 organic solar cells via oghmanano software optimisation," in *2023 3rd International Conference on Smart Generation Computing, Communication and Networking (SMART GENCON)*, Dec. 2023, pp. 1–6, doi: 10.1109/SMARTGENCON60755.2023.10442773.
[30] A. K. K. Kyaw *et al.*, "Improved light harvesting and improved efficiency by insertion of an optical spacer (ZnO) in solution-processed small-molecule solar cells," *Nano Letters*, vol. 13, no. 8, pp. 3796–3801, Aug. 2013, doi: 10.1021/nl401758g.
[31] S. Ben Dkhil *et al.*, "Interplay of optical, morphological, and electronic effects of ZnO optical spacers in highly efficient polymer solar cells," *Advanced Energy Materials*, vol. 4, no. 18, Dec. 2014, doi: 10.1002/aenm.201400805.
[32] S. Lattante, "Electron and hole transport layers: their use in inverted bulk heterojunction polymer solar cells," *Electronics*, vol. 3, no. 1, pp. 132–164, Mar. 2014, doi: 10.3390/electronics3010132.
[33] C. Guillén and J. Herrero, "TCO/metal/TCO structures for energy and flexible electronics," *Thin Solid Films*, vol. 520, no. 1, pp. 1–17, Oct. 2011, doi: 10.1016/j.tsf.2011.06.091.

BIOGRAPHIES OF AUTHORS

Karthika Krishnakumar is a research scholar at Manav Rachna International Institute of Research and Studies (MRIIRS), Faridabad, Haryana, India. Her research expertise in thin-film solar cells. Currently, she is working on organic solar cells. She is also working as a research assistant at Manav Rachna International Institute of Research and Studies. She did B.Sc. in electronics from St. Thomas College under Calicut University, Kerala, India, and M.Sc. in electronics from Jamia Millia Islamia, New Delhi, India. She can be contacted at email: karthikakrishnakumar18752@gmail.com.

Dr. Ashish Grover presently working as associate professor at Manav Rachna International Institute of Research and Studies, Faridabad, Haryana, India from August 2010. She has also worked at ApeeJay College of Engineering, Sohna, Gurgaon, Haryana, India. She has published research papers in national and international journals. Her research areas include electrical machines, power systems, power electronics, sustainable energy, electric vehicles, automation, and OT. She is a lifetime member in Institutions of Engineer's and a lifetime member in Indian Society of Technical Education. She can be contacted at email: ashishgrover.fet@mriu.edu.in.

Prof. (Dr.) Pardeep Kumar is a professor, pro-vice chancellor, and dean at Manav Rachna International Institute of Research and Studies, Faridabad has 30 years of teaching and research experience. He did his B.Sc. (Hons.) in physics from Delhi University (India), M.Sc. from Jamia Millia Islamia, and Ph.D. from National Physical Laboratory (India). He has authored 6 books and published 29 research papers. He is a life member of Indian Physics Association and Meteorological Society of India. His research areas include laser photoacoustic, characterization of materials, ECR etching, and soi-gel glass materials. He can be contacted at email: pvc.pk@mriu.edu.in.